HHS Public Access

Author manuscript

J Am Chem Soc. Author manuscript; available in PMC 2023 November 27.

Published in final edited form as:

J Am Chem Soc. 2022 November 23; 144(46): 21278–21286. doi:10.1021/jacs.2c08989.

Nickel Catalysis via S_H2 Homolytic Substitution: The Double Decarboxylative Cross-Coupling of Aliphatic Acids

Artem V. Tsymbal[†],

Merck Center for Catalysis at Princeton University, Princeton, New Jersey 08544, United States

Lorenzo Delarue Bizzini[†],

Merck Center for Catalysis at Princeton University, Princeton, New Jersey 08544, United States

David W. C. MacMillan

Merck Center for Catalysis at Princeton University, Princeton, New Jersey 08544, United States

Abstract

Cross-coupling platforms are traditionally built around a sequence of closed-shell steps, such as oxidative addition, transmetalation, and reductive elimination. Herein, we describe a dual photo/nickel catalytic manifold that performs cross-coupling via a complementary sequence involving free radical generation, radical sorting via selective binding to a Ni(II) center, and bimolecular homolytic substitution (S_H2) at a high-valent nickel–alkyl complex. This catalytic manifold enables the hitherto elusive cross-coupling of diverse aliphatic carboxylic acids to generate valuable $C(sp^3)$–$C(sp^3)$-products. Notably, the powerful S_H2 mechanism provides general access to sterically encumbered quaternary carbon centers, addressing a long-standing challenge in fragment coupling chemistry.

Graphical Abstract

Corresponding Author: David W. C. MacMillan – Merck Center for Catalysis at Princeton University, Princeton, New Jersey 08544, United States; dmacmill@princeton.edu.

[†]A.V.T. and L.D.B. contributed equally.

Complete contact information is available at: https://pubs.acs.org/10.1021/jacs.2c08989

Accession Codes

CCDC 2144755 contains the supplementary crystallographic data for this paper. These data can be obtained free of charge via www.ccdc.cam.ac.uk/data_request/cif, or by emailing data_request@ccdc.cam.ac.uk, or by contacting The Cambridge Crystallographic Data Centre, 12 Union Road, Cambridge CB2 1EZ, UK; fax: +44 1223 336033.

The authors declare the following competing financial interest(s): D. W. C. M. declares a competing financial interest with respect to the integrated photoreactor.

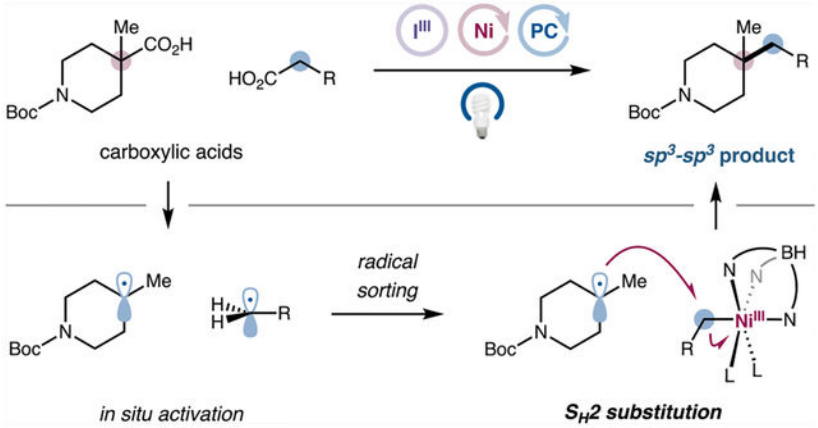

INTRODUCTION

Transition-metal-catalyzed cross-coupling methods have enabled the rapid advancement of disciplines that rely on the assembly of complex molecular architectures, including chemistry, pharmacology, material science, and biology.[1–3] Although traditional cross-coupling approaches construct bonds between organic electrophiles and organometallic nucleophiles, the emergence of multicatalytic platforms, such as metallaphotoredox catalysis,[4,5] has extended this fragment-coupling logic to the direct coupling of native functionalities, such as chlorides,[6] alcohols,[7,8] carboxylic acids,[8–11] and C–H bonds[12,13] via open-shell pathways. Among these building blocks, carboxylic acids hold a privileged position, as they are widely commercially available, structurally diverse, benchtop stable, relatively nontoxic, and ubiquitous in both natural products and pharmaceutical agents.[14–16] Indeed, aliphatic acids have been productively engaged in numerous metallaphotoredox transformations, including alkylation,[8,9] arylation,[10,17] amination,[18] and trifluoromethylation.[19] Despite these advances, however, direct metal-catalyzed cross-coupling between two distinct carboxylic acids to generate C(sp^3)–C(sp^3) products remains elusive.[20]

It is now well understood that the likelihood that a small-molecule therapeutic candidate will successfully progress through clinical trials is positively correlated with the proportion of saturated sp^3-carbon atoms in the molecule.[21,22] Moreover, incorporation of quaternary carbon centers onto a cyclic framework provides conformational rigidity, leading to improved pharmacokinetic properties.[23,24] However, applying the machinery of traditional cross-coupling platforms to the construction of C(sp^3)–C(sp^3)-bonds is innately challenging, due to the slow rates of reductive elimination from intermediate dialkyl metal complexes and their proclivity to undergo side reactions,[25] such as β-hydride elimination, metal–carbon bond scission, and oxidation of electron-rich alkyl groups to carbocations. Thus, despite concerted efforts in base-metal catalysis over the past two decades,[26] the general use of cross-coupling protocols to forge C(sp^3)–C(sp^3) bonds remains a daunting task, particularly in the context of constructing quaternary carbon centers.[27,28]

A conceptually appealing alternative to conventional coupling methods is to achieve cross-coupling via the recombination of free alkyl radicals. To date, kinetic obstacles have hindered the widespread development of this fundamental reactivity mode (Figure 1A). Because reactions between free radicals are diffusion controlled, they lead to mixtures of homodimers and cross-coupled products in cases where both radicals have similar lifetimes and are generated at the same rate. Hence, to reach practical selectivity, one of the radicals must be stabilized to have a significantly lower self-termination rate; this requirement substantially narrows the scope of such transformations.[29–31] Moreover, encounters between alkyl radicals are intrinsically unselective and, aside from cross-coupled products, lead to considerable amounts of radical disproportionation byproducts.[32]

We anticipated that a solution to the challenges of both C(sp^3)–C(sp^3)-reductive elimination and free radical recombination could be accomplished through a new manifold encompassing free radical generation, followed by selective radical-to-metal binding, and bimolecular homolytic substitution (S_H2) (Figure 1B). It is well established that the strength of the metal-alkyl bond decreases as the degree of alkyl group substitution increases.[33] We recognized that this thermodynamic trend could be harnessed to achieve radical sorting in reaction mixtures (Figure 2A). Thus, we envisioned a metal system designed to selectively capture methyl and primary alkyl radicals, leaving hindered secondary and tertiary radicals unbound. This selective colligation to the metal center would serve to decrease the concentration of the primary radical and produce metal alkyl species. Consequently, the S_H2 reaction between the persistent metal alkyl complex and a transient tertiary radical en route to cross-coupled product would become a major kinetic channel, similar to the persistent radical effect. Although the key bimolecular homolytic substitution (S_H2) step has been known for several decades,[34] S_H2 at saturated carbon centers has been rarely proposed in the chemical literature.[35,36] It was primarily identified as a reactivity mode of cobalt(III) alkyl complexes,[37] including cobalamin cofactors in radical methyl-transferases,[38] for which the S_H2 methylation step was determined to proceed extremely rapidly (~10^8 s^{-1}).[39]

Building on these design principles, our group recently disclosed a metallaphotoredox platform for cross-coupling of alkyl bromides and redox-active esters via iron porphyrin catalysis.[40] Notably, the iron porphyrin protocol provided robust access to sterically congested quaternary C(sp^3) centers. Inspired by this finding, we questioned whether this strategy could enable selective cross-coupling between two substrates bearing identical functionalities, specifically carboxylic acids (Figure 1C). We envisioned that both acids could be simultaneously transformed into free radicals, while coupling cross-selectivity would be achieved through metal-mediated radical sorting. Recently, in a series of stoichiometric experiments, the Sanford lab proposed S_H2 as a reactivity mode for high-valent Ni alkyl trispyrazolylborate complexes.[36] Along these lines, we sought to explore whether a nickel scorpionate scaffold could provide a general S_H2-catalysis platform complementary to previously established cobalt and iron porphyrin systems.

RESULTS AND DISCUSSION

A plausible mechanism for the proposed double decarboxylative cross-coupling reaction is outlined in Figure 2B. A carboxylic acid **1** is envisioned to undergo facile ligand exchange

with a pre-formed iodomesitylene carboxylate **2**, producing a mixture of heteroleptic and homoleptic I(III) carboxylates **3**.[41] For clarity, only heteroleptic dicarboxylate is shown here [the carboxylate exchange at I(III) centers was observed by NMR spectroscopy; see Figure S2 for a more complete picture]. Regardless of the exact composition of this mixture, all of these hypervalent iodine species are ultimately expected to lead to alkyl free radicals. Concurrently, a photocatalyst—thioxanthone (TXO) or 2,4,5,6-tetrakis(9*H*-carbazol-9-yl)isophthalonitrile (4CzIPN)—undergoes irradiation with UV or visible light, respectively, to access a long-lived, high-energy triplet state (2.8 and 2.6 eV, respectively).[42,43] The photoexcited state is expected to transfer the triplet energy (see Figures S10 and S11 for Stern–Volmer fluorescence quenching studies and Table S32 for control experiments. Alternative photoredox activation pathways are available for 4CzIPN; see Pages S39 and S40 for discussion) to hypervalent iodine(III) species **3**, resulting in homolysis of both I–O bonds to form carboxyl radicals. The latter are known to rapidly extrude CO_2, yielding free alkyl radicals **4** and **5**.[44] At this stage, Ni(II) complex **6** would presumably selectively capture the less substituted alkyl radical, **4**, generating Ni(III) alkyl complex, **7**. The resulting organometallic intermediate is proposed to undergo S_H2 homolytic substitution with the more substituted alkyl radical, **5**, yielding the desired cross-coupled product **8** and regenerating the Ni(II) catalyst **6** (vide infra).

We began our investigations into the proposed reaction by examining the coupling between medicinally relevant *N*-tosylisonipecotic acid and commercial iodomesitylene diacetate as the preactivated form of acetic acid (see Tables S1–S31 for details). All reactions were performed in commercial photoreactors[45] to ensure reproducibility of the data and to facilitate eventual transfer of the reaction protocols to medicinal chemistry settings. Gratifyingly, through the optimization campaign, we observed that the reaction could be catalyzed using benchtop-stable, commercially available nickel(II) acetylacetonate $Ni(acac)_2$ as the metal source and potassium tri(3,5-dimethyl-1-pyrazolyl)borohydride (K[Tp*]) as the ligand (Tables S1–S3 and S14). The intermediate alkyl radicals could be generated via direct photolysis of aryliodine-(III) carboxylates using 365 nm UV light; however, we found that the use of a triplet sensitizer drastically expands the scope of the reaction (Tables S15 and S16). Thus, we developed two experimental protocols that differ in both the light source and photosensitizer: the first employs 365 nm UV light in combination with TXO as a sensitizer (Table 1) and the second uses 450 nm light with 4CzIPN (Page S136). The latter visible light protocol was necessary for rare examples when the substrate decomposes upon UV irradiation. Both protocols delivered the desired methylated product in good yields: 84 and 79%, respectively, on a 1 mmol scale. Unreacted secondary carboxylic acid, as well as protodecarboxylation and decarboxylative olefination side products, accounted for the remainder of the mass balance (Table S19). The differences in yields of the UV and visible light protocols could be attributed to the difference in the photostability of the sensitizers, the difference in the alkyl radical generation rates, and the ability of 4CzIPN (unlike TXO) to engage in electron-transfer processes with the starting materials (see discussion on Pages S39 and S40) or intermediate alkyl radicals. Notably, the reaction was amenable to a range of solvents, from toluene to wet dimethylsulfoxide; benchtop dimethyl carbonate (Me_2CO_3) was identified as the optimal solvent (Table S25).

Control experiments showed that all components of the reaction protocol—nickel source, scorpionate K[Tp*] ligand, sensitizers, and light source—are required for optimal performance (Tables 1 and S32). The nickel catalyst played an important role in mediating both reaction efficiency and cross-coupling selectivity. Thus, under nickel-catalyzed conditions, the yield of the cross-coupled product supersedes statistical expectations for various loadings of $MesI(OAc)_2$ (Table S28), in line with the proposed radical sorting principle. In contrast, uncatalyzed encounters of the free radicals were not synthetically valuable even when an immense excess of $MesI(OAc)_2$ was used (Table S29). Furthermore, the $Ni(acac)_2$/K[Tp*] system also dramatically improved the ratio of the cross-coupled product to the homo-recombination product. In fact, under nickel-catalyzed conditions, the 2°–2° homo-recombination product was observed only in trace amounts (<1%) (Tables S19 and S28). These results strongly support the capacity of the designed nickel catalytic platform to achieve radical sorting and subsequent streamlining of the cross-coupling reactivity.

With the optimized experimental protocols in hand, we sought to evaluate the scope of the decarboxylative methylation reaction. As demonstrated in Figure 3, these protocols were found to be general and robust, with remarkable functional group tolerance and applicability to a wide range of medicinally relevant carboxylic acids (17 additional examples can be found in Figure S3). Primary acids bearing bio-relevant heterocyclic rings, such as pyridine, benzotriazole, and 1,2,4-oxadiazole, provided corresponding methylated products in good yields (**9** and **10**, 67 and 80%, respectively).

A broad spectrum of secondary acids was successfully engaged in the $C(sp^3)$–$C(sp^3)$ cross-coupling reaction. Open-chain benzylic and aliphatic acids (**11–13**, 57–90% yields) afforded methylated products in good to excellent yields, revealing β-lactams as well as protected and unprotected alcohol groups to be well tolerated. The compatibility of free alcohols with the reaction is of particular importance for medicinal chemistry programs, as it removes the need to protect ubiquitous alcohol functionalities. We further established that the methylation protocol is efficient for a diverse range of cyclic secondary acids, including azaspiro[3.3]heptane (**14**, 70% yield), β-amidocyclopentane (**15**, 70% yield), pyrrolidine (**16**, 83% yield), piperidines 2014 including those bearing unprotected alcohols and 1,2,3-triazole functionality (**17–19**, 66–85% yields)—and nortropane (**20**, 81% yield). Notably, the successful cross-coupling of acids bearing electron-withdrawing α-F (**17**) and α-CF_3 (**13**) groups demonstrates that electrophilic radicals are capable of efficient S_H2 alkylation.

The cross-coupling protocol is applicable to a wide range of structurally unbiased tertiary acids, providing access to synthetically challenging quaternary carbon products. As shown in Figure 3, cyclic tertiary acids of different ring sizes, including cyclopropyl (**21**, 68% yield), azetidine with a pendant alkene moiety (**22**, 73% yield), and pyrrolidine (**23–24**, 83–86% yields) deliver quaternary methylated products in good to excellent yields. Furthermore, a homobenzylic cyclohexyl carboxylic acid, prone to metal-mediated β-hydrogen elimination and bearing both an unprotected alcohol and an aryl bromide, was methylated with excellent efficiency (**25**, 91% yield); this result demonstrates the power of the method to effectively modify the types of highly functionalized building blocks that are generally used in discovery chemistry campaigns. In addition, the bridgehead positions of

bicyclo[4.4.0]decane (**26**, 74% yield), adamantane (**27**, 59% yield), and bicyclo[2.2.2]octane (**28**, 40% yield) were methylated in good yields, illustrating the applicability of this chemistry to fused and caged polycyclic systems. Finally, an open-chain tertiary carboxylic acid, Gemfibrozil, was found to undergo efficient methylation (**29**, 78% yield).

Next, we turned our attention to α-amino and oxyacids. Exposure of these substrates to the reaction conditions afforded the corresponding methylated products in good yields (**30–33**, 61–81% yields), demonstrating that highly nucleophilic radicals are capable of undergoing S_H2 alkylation. These results, taken together with the successful incorporation of electron-withdrawing fluorinated groups (**13** and **17**), reveal that radical polarity has minimal influence on reaction performance. Finally, it is notable that the chemistry tolerates the presence of an isoxazole ring (31), a motif that often poses a challenge in metal-catalyzed cross-couplings.[46,47]

To further demonstrate the utility of the decarboxylative methylation protocol for the late-stage functionalization of biologically relevant systems, we examined the reaction in the context of a range of complex medicinal agents and natural products (**34–39**). Remarkably, both Artesunate, containing a peroxide ketal scaffold, and Gibberellin A3, containing two unprotected allylic alcohol groups, were transformed into **34** and **38** in 44 and 76% yield, respectively, illustrating a level of functional group tolerance that is unusual for a cross-coupling reaction. Additionally, the successful methylation of Ambrisentan (**36**, 89% yield), which bears an α-diphenyl fragment, demonstrates that this technology can furnish C–C bonds even in highly sterically crowded settings.

Having established the scope of this reaction with acetic acid as the small-alkyl source, we now turned our attention to achieving cross-coupling with other small-alkyl sources (Figure 4). The small-alkyl carboxylic acid used in excess could be conveniently preactivated to the corresponding iodomesitylene dicarboxylate via mixing with MesIO in the presence of $MgSO_4$. The resulting I(III) reagents were formed quantitatively after filtering off the drying agent and subjected to the reaction conditions without any purification. Alternatively, the reaction could be performed with the same efficiency without this preactivation step simply by combining both carboxylic acids and MesIO in the reaction mixture (see Table S35 and Figure S4). These protocols were used to efficiently access isotopically labeled CD_3 (40, 82% yield) and ^{13}C-methyl (**41**, 71% yield) products. The protocols are also amenable to substituted acetic acids (**42–44**, 42–58% yields) and propionic acids (**45–46**, 45–74% yields). Small alkyl groups were also installed to construct quaternary carbon centers (**47–49**, 44–47% yields).

We next investigated the mechanistic aspects of the nickel catalytic cycle. First, we strove to confirm that the C–C bond formation step does indeed involve the nickel species. However, variable time normalization kinetic analysis revealed that for the UV-light protocol the rate-determining step of the overall transformation is photosensitization of the hypervalent iodine species, and reaction rate does not depend on the concentration of nickel catalyst (see Section 11 of the Supporting Information). Thus, we turned to stereochemical probing and subjected β-amino acid **50** to several methylation conditions to observe diastereomeric mixtures of *trans*/*cis* **15** (Figure 5A). The nickel-free control

experiment afforded the cross-coupled product in 34% yield and 1.5:1 d.r., presumably through uncatalyzed recombination of free alkyl radicals. Introduction of the nickel catalyst and potassium tri(1-pyrazolyl)borohydride K[Tp] ligand increased the reaction yield to 63% and improved the product d.r. to 2.4:1. Using the optimal ligand, K[Tp*], we observed a further increase in both reaction yield (81%) and d.r. (3.0:1). Changes in the reaction yield and d.r. upon variation of ligand strongly indicate that nickel species are directly involved in the C–C bond formation step.

We then sought to probe the intermediacy of low-valent nickel species in the reaction. Conventionally, nickel-catalyzed cross-coupling reactions are proposed to proceed via low-valent Ni(0) and Ni(I) complexes.[48,49] However, cyclic voltammetry (Figures S7–S9) suggests that these species are unlikely to be present under the reaction conditions, because $MesI(OAc)_2$, which is used in super-stoichiometric quantities, is sufficiently oxidizing ($E_i^{red} = -0.82$ V vs saturated calomel electrode, SCE) to convert Ni(I) species ($E_i^{red} = -1.74$ V vs SCE) into Ni(II). Moreover, the general compatibility of substrates bearing reductively unstable moietiessuch as isoxazole (**31**), 1,2,4-oxadiazole (**9**), and alkyl peroxide (**34**)—is additional evidence against the involvement of low-valent metal complexes. To further examine this issue, we subjected *N*-tosylisonipecotic acid, **51**, to the standard methylation protocol in the presence of excess quantities of activated aryl halides **53** and **54** (Figure 5B). Low-valent nickel species are known to undergo rapid oxidative addition into Ar–Br and especially Ar–I bonds.[50,51] Thus, deterioration of the reaction yield and consumption of the halides may indicate the presence of Ni(0) or Ni(I) species. Notably, however, addition of **53** or **54** did not decrease the yield of the methylated product; moreover, these aryl halides were fully recovered after reaction completion, providing further evidence against the intermediacy of Ni(0) and Ni(I) species in the formation of cross-coupled products.

To investigate nickel speciation upon irradiation, we turned to in situ photo electron paramagnetic resonance (photoEPR) spectroscopy (Figure 5C). A solution containing $MesI(OAc)_2$, isolated Tp*Ni(OAc) complex **55** (see Supporting Information Section 7),[52] and TXO in benzene was EPR-silent in the dark, demonstrating that the hypervalent iodine reagent does not thermally oxidize the Ni(II) complex. UV–vis spectral analysis further corroborated this finding: the addition of $MesI(OAc)_2$ to an acidified toluene solution of Tp*Ni(OAc) complex **55** did not lead to the appearance of new spectral features (Figure S6). However, upon irradiation with 365 nm UV light, a sole EPR signal, a singlet with $g = 2.17$, emerged (Figure S12). A significant deviation of the g value from that of a free electron ($g_e = 2.0023$) is indicative of a spin system centered at a transition-metal atom. Control experiments demonstrated that both $MesI(OAc)_2$ and Tp*Ni(OAc) **55** are required to detect the signal (Figure S12). In the absence of TXO, the same signal was registered, although of lower intensity. The latter is consistent with the fact that $MesI(OAc)_2$ is directly photolyzed by 365 nm light and TXO functions as a triplet sensitizer in the system. Importantly, continuous irradiation of the sample was essential; when the light source was turned off, the signal disappeared within seconds, implying that the observed paramagnetic species are labile and rapidly decompose without continuous generation of methyl radicals. Based on these results, we tentatively assigned the signal to the product of methyl radical capture by Tp*Ni(OAc)—the low-spin d^7-Ni(III)–Me complex **56a**. Next, to

support this signal assignment, we conducted analogous spectroscopic experiments with a different methyl radical source, di-*tert*-butyl peroxide. Indeed, the identical EPR signal (g = 2.17) was registered in this case, corroborating the proposed nature of the paramagnetic species, **56a** (see Figure S17 for low-temperature photoEPR spectrum of **56a**). Furthermore, the same EPR signal was detected in a methylation reaction mixture (Figure S16), and a subsequent quantitative EPR experiment revealed that 1.0% of the initial Tp*Ni(OAc) **55** was converted into the Ni(III)–Me complex **56a** upon photolysis of MesI(OAc)$_2$. Reactivity of this Ni(III)–Me complex, 56a, was studied using density functional theory (DFT). These investigations established that **56a** undergoes the proposed S_H2 step with a variety of alkyl radicals at near-diffusion rates (Figure S25) to yield corresponding methylated products.

Finally, we subjected a series of iodomesitylene dicarboxylates to the same photoEPR experiments to examine the radical sorting design principle (Figure 5D). Aside from MesI(OAc)$_2$, only MesI(O$_2$CEt)$_2$ led to a detectable EPR signal (g = 2.19, Figure S15), which was assigned to Ni(III)–Et **56b** complex by analogy. The identical trend was observed when the EPR spectra were recorded at 10 K from frozen toluene glass samples (Figures S17–S20). These observations are consistent with our theoretical DFT estimates of Ni–C BDFEs: alkyl radical binding to Tp*Ni(OAc) **55** is thermodynamically favored only for methyl and ethyl radicals (Figures S18). Combined, these experimental and computational data demonstrate that high-valent nickel chemistry can provide a generic platform for sequential radical-to-metal binding and S_H2 substitution.

CONCLUSIONS

We disclose herein a multicatalytic platform that enables the cross-coupling of aliphatic carboxylic acids. In situ activation of acids in the form of iodoarene carboxylates and subsequent photosensitization of the hypervalent iodine species provides generic access to alkyl radicals. The designed Ni(II) scorpionate platform subsequently intercepts the alkyl radicals with a predictable selectivity. Eventually, C–C bonds are furnished via an underutilized bimolecular homolytic substitution (S_H2) mechanism. This catalytic platform provides general access to sterically encumbered quaternary carbon centers and demonstrates a level of functional group tolerance that is unusual for a cross-coupling reaction. Furthermore, mechanistic studies suggest that the S_H2 step occurs at a Ni(III) alkyl scorpionate complex, illustrating that this mechanism is not limited to porphyrin-based systems and thus might be more abundant than previously anticipated. Work on further application of this platform is underway in our lab.

Supplementary Material

Refer to Web version on PubMed Central for supplementary material.

ACKNOWLEDGMENTS

The authors are grateful for financial support provided by the National Institute of General Medical Sciences (NIGMS), the NIH (under Award R35GM134897-03), the Princeton Catalysis Initiative, and kind gifts from Merck, Janssen, BMS, Genentech, Celgene, and Pfizer. The content is solely the responsibility of the authors and does not necessarily represent the official views of NIGMS. A.V.T. acknowledges Princeton University, E. Taylor, and the Taylor family for an Edward C. Taylor Fellowship. L.D.B. acknowledges Swiss National Science Foundation

(P2BSP2_188129) for funding. The authors thank I. Pelczer and K. Conover for assistance with NMR spectroscopy, J. Eng for assistance with EPR spectroscopy and HRMS analysis, P. Jeffrey for performing X-ray analysis, C. Gould for assistance with CV analysis, and Rebecca Lambert for assistance in the preparation of this manuscript.

REFERENCES

(1). de Meijere A; Bräse S; Oestreich M Metal Catalyzed Cross-Coupling Reactions and More; Wiley-VCH Verlag, 2013.

(2). Campeau LC; Hazari N Cross-Coupling and Related Reactions: Connecting Past Success to the Development of New Reactions for the Future. Organometallics 2019, 38, 3–35. [PubMed: 31741548]

(3). Buskes MJ; Blanco M-J; Sestelo JP; Sarandeses LA Impact of Cross-Coupling Reactions in Drug Discovery and Development. Molecules 2020, 25, 3493. [PubMed: 32751973]

(4). Twilton J; Le CC; Zhang P; Shaw MH; Evans RW; MacMillan DWC The Merger of Transition Metal and Photocatalysis. Nat. Rev. Chem 2017, 1, 52.

(5). Chan AY; Perry IB; Bissonnette NB; Buksh BF; Edwards GA; Frye LI; Garry OL; Lavagnino MN; Li BX; Liang Y; Mao E; Millet A; Oakley J. v.; Reed NL; Sakai HA; Seath CP; MacMillan DWC Metallaphotoredox: The Merger of Photoredox and Transition Metal Catalysis. Chem. Rev 2022, 122, 1485–1542. [PubMed: 34793128]

(6). Sakai HA; Liu W; Le C; MacMillan DWC Cross-Electrophile Coupling of Unactivated Alkyl Chlorides. J. Am. Chem. Soc 2020, 142, 11691–11697. [PubMed: 32564602]

(7). Dong Z; MacMillan DWC Metallaphotoredox-Enabled Deoxygenative Arylation of Alcohols. Nature 2021, 598, 451–456. [PubMed: 34464959]

(8). Sakai HA; MacMillan DWC Nontraditional Fragment Couplings of Alcohols and Carboxylic Acids: C(sp^3)-C(sp^3) Cross-Coupling via Radical Sorting. J. Am. Chem. Soc 2022, 144, 6185–6192. [PubMed: 35353531]

(9). Johnston CP; Smith RT; Allmendinger S; MacMillan DWC Metallaphotoredox-Catalysed sp^3-sp^3 Cross-Coupling of Carboxylic Acids with Alkyl Halides. Nature 2016, 536, 322–325. [PubMed: 27535536]

(10). Zuo Z; MacMillan DWC Decarboxylative Arylation of α-Amino Acids via Photoredox Catalysis: A One-Step Conversion of Biomass to Drug Pharmacophore. J. Am. Chem. Soc 2014, 136, 5257–5260. [PubMed: 24712922]

(11). Zuo Z; Ahneman DT; Chu L; Terrett JA; Doyle AG; MacMillan DWC Merging Photoredox with Nickel Catalysis: Coupling of Carboxyl sp^3-Carbons with Aryl Halides. Science 2014, 345, 437–440. [PubMed: 24903563]

(12). Perry IB; Brewer TF; Sarver PJ; Schultz DM; DiRocco DA; MacMillan DWC Direct Arylation of Strong Aliphatic C–H Bonds. Nature 2018, 560, 70–75. [PubMed: 30068953]

(13). Vasilopoulos A; Krska SW; Stahl SS C(sp^3)–H Methylation Enabled by Peroxide Photosensitization and Ni-Mediated Radical Coupling. Science 2021, 372, 398–403. [PubMed: 33888639]

(14). Ertl P An Algorithm to Identify Functional Groups in Organic Molecules. J. Cheminf 2017, 9, 36.

(15). Ertl P; Schuhmann T A Systematic Cheminformatics Analysis of Functional Groups Occurring in Natural Products. J. Nat. Prod 2019, 82, 1258–1263. [PubMed: 30933507]

(16). Henkel T; Brunne RM; Müller H; Reichel F Statistical Investigation into the Structural Complementarity of Natural Products and Synthetic Compounds. Angew. Chem., Int. Ed 1999, 38, 643–647.

(17). Zuo Z; Cong H; Li W; Choi J; Fu GC; MacMillan DWC Enantioselective Decarboxylative Arylation of α-Amino Acids via the Merger of Photoredox and Nickel Catalysis. J. Am. Chem. Soc 2016, 138, 1832–1835. [PubMed: 26849354]

(18). Liang Y; Zhang X; MacMillan DWC Decarboxylative sp^3 C-N Coupling via Dual Copper and Photoredox Catalysis. Nature 2018, 559, 83–88. [PubMed: 29925943]

(19). Kautzky JA; Wang T; Evans RW; MacMillan DWC Decarboxylative Trifluoromethylation of Aliphatic Carboxylic Acids. J. Am. Chem. Soc 2018, 140, 6522–6526. [PubMed: 29754491]

(20). While this manuscript was in preparation an electrochemical nickel-catalyzed cross-coupling of redox-active esters was disclosed:Zhang B; Gao Y; Hioki Y; Oderinde MS; Qiao JX; Rodriguez KX; Zhang H-J; Kawamata Y; Baran PS Ni-Electrocatalytic Csp^3-Csp^3 Doubly Decarboxylative Coupling. Nature 2022, 606, 313–318. [PubMed: 35381598]

(21). Lovering F; Bikker J; Humblet C Escape from Flatland: Increasing Saturation as an Approach to Improving Clinical Success. J. Med. Chem 2009, 52, 6752–6756. [PubMed: 19827778]

(22). Lovering F Escape from Flatland 2: Complexity and Promiscuity. MedChemComm 2013, 4, 515–519.

(23). Talele TT Opportunities for Tapping into Three-Dimensional Chemical Space through a Quaternary Carbon. J. Med. Chem 2020, 63, 13291–13315. [PubMed: 32805118]

(24). Talele TT Natural-Products-Inspired Use of the GemDimethyl Group in Medicinal Chemistry. J. Med. Chem 2017, 61, 2166–2210. [PubMed: 28850227]

(25). Hartwig JF Organotransition Metal Chemistry: From Bonding to Catalysis; University Science Books: Sausalito, CA, 2010; p 1127.

(26). Choi J; Fu GC Transition Metal-Catalyzed Alkyl-Alkyl Bond Formation: Another Dimension in Cross-Coupling Chemistry. Science 2017, 356, No. eaaf7230.

(27). Xue W; Jia X; Wang X; Tao X; Yin Z; Gong H Nickel-Catalyzed Formation of Quaternary Carbon Centers Using Tertiary Alkyl Electrophiles. Chem. Soc. Rev 2021, 50, 4162–4184. [PubMed: 33533345]

(28). Jana R; Pathak TP; Sigman MS Advances in Transition Metal (Pd, Ni, Fe)-Catalyzed Cross-Coupling Reactions Using Alkyl-Organometallics as Reaction Partners. Chem. Rev 2011, 111, 1417–1492. [PubMed: 21319862]

(29). Leifert D; Studer A The Persistent Radical Effect in Organic Synthesis. Angew. Chem., Int. Ed 2019, 59, 74–108.

(30). Sun Z; Tang B; Liu KKC; Zhu HY Direct Photochemical Cross-Coupling between Aliphatic Acids and BF_3K Salts. Chem. Commun 2020, 56, 1294–1297.

(31). Fischer H The Persistent Radical Effect: A Principle for Selective Radical Reactions and Living Radical Polymerizations. Chem. Rev 2001, 101, 3581–3610. [PubMed: 11740916]

(32). Gibian MJ; Corley RC Organic Radical-Radical Reactions. Disproportionation vs. Combination. Chem. Rev 1973, 73, 441–464.

(33). Simoes JAM; Beauchamp JL Transition Metal–Hydrogen and Metal–Carbon Bond Strengths: The Keys to Catalysis. Chem. Rev 1990, 90, 629–688.

(34). Ingold KU; Roberts BP Free-Radical Substitution Reactions. Bimolecular Homolytic Substitutions (S_H2 Reactions) at Saturated Multivalent Atoms, 1st ed.; John Wiley & Sons Inc., 1971.

(35). Walton JC Homolytic Substitution: A Molecular Ménage à Trois. Acc. Chem. Res 1998, 31, 99–107.

(36). Bour JR; Ferguson DM; McClain EJ; Kampf JW; Sanford MS Connecting Organometallic Ni(III) and Ni(IV): Reactions of Carbon-Centered Radicals with High-Valent Organonickel Complexes. J. Am. Chem. Soc 2019, 141, 8914–8920. [PubMed: 31136162]

(37). Johnson MD Bimolecular Homolytic Displacement of Transition-Metal Complexes from Carbon. Acc. Chem. Res 2002, 16, 343–349.

(38). Zhang Q; van der Donk WA; Liu W Radical-Mediated Enzymatic Methylation: A Tale of Two SAMS. Acc. Chem. Res 2012, 45, 555–564. [PubMed: 22097883]

(39). Wang Y; Begley TP Mechanistic Studies on CysS - A Vitamin B_{12}-Dependent Radical SAM Methyltransferase Involved in the Biosynthesis of the Tert-Butyl Group of Cystobactamid. J. Am. Chem. Soc 2020, 142, 9944–9954. [PubMed: 32374991]

(40). Liu W; Lavagnino MN; Gould CA; Alcázar J; MacMillan DWC A Biomimetic S_H2 Cross-Coupling Mechanism for Quaternary sp^3-Carbon Formation. Science 2021, 374, 1258–1263. [PubMed: 34762491]

(41). Kiyokawa K; Watanabe T; Fra L; Kojima T; Minakata S Hypervalent Iodine(III)-Mediated Decarboxylative Ritter-Type Amination Leading to the Production of α-Tertiary Amine Derivatives. J. Org. Chem 2017, 82, 11711–11720. [PubMed: 28603990]

(42). Romero NA; Nicewicz DA Organic Photoredox Catalysis. Chem. Rev 2016, 116, 10075–10166. [PubMed: 27285582]

(43). Teets TS; Wu Y; Kim D Photophysical Properties and Redox Potentials of Photosensitizers for Organic Photoredox Transformations. Synlett 2022, 33, 1154–1179.

(44). Hilborn JW; Pincock JA Rates of Decarboxylation of Acyloxy Radicals Formed in the Photocleavage of Substituted 1-Naphthylmethyl Alkanoates. J. Am. Chem. Soc 1991, 113, 2683–2686.

(45). Le CC; Wismer MK; Shi ZC; Zhang R; Conway D. v.; Li G; Vachal P; Davies IW; MacMillan DWC A General Small-Scale Reactor to Enable Standardization and Acceleration of Photocatalytic Reactions. ACS Cent. Sci 2017, 3, 647–653. [PubMed: 28691077]

(46). Ahneman DT; Estrada JG; Lin S; Dreher SD; Doyle AG Predicting Reaction Performance in C-N Cross-Coupling Using Machine Learning. Science 2018, 360, 186–190. [PubMed: 29449509]

(47). Yu S; Tang G; Li Y; Zhou X; Lan Y; Li XA An Aminating Reagent Leading to Bifunctionality for Both C(sp^3)–H and C(sp^2)–H under Rhodium (III) Catalysis. Angew. Chem., Int. Ed 2016, 128, 8838–8842.

(48). Diccianni JB; Diao T Mechanisms of Nickel-Catalyzed Cross-Coupling Reactions. Trends Chem. 2019, 1, 830–844.

(49). Diccianni J; Lin Q; Diao T Mechanisms of Nickel-Catalyzed Coupling Reactions and Applications in Alkene Functionalization. Acc. Chem. Res 2020, 53, 906–919. [PubMed: 32237734]

(50). Till NA; Oh S; MacMillan DWC; Bird MJ The Application of Pulse Radiolysis to the Study of Ni(I) Intermediates in Ni-Catalyzed Cross-Coupling Reactions. J. Am. Chem. Soc 2021, 143, 9332–9337. [PubMed: 34128676]

(51). Greaves ME; Johnson Humphrey ELB; Nelson DJ Reactions of Nickel(0) with Organochlorides, Organobromides, and Organoiodides: Mechanisms and Structure/Reactivity Relationships. Catal. Sci. Technol 2021, 11, 2980–2996.

(52). Tp*Ni(OAc) complex 55 has been reported previously:Hikichi S; Sasakura Y; Yoshizawa M; Ohzu Y; Moro-oka Y; Akita M Selective Synthesis, Characterization, and Configurational Flexibility of the Coordinatively Unsaturated Metal Center of Half-Sandwich Type Complexes with the Less-Hindered Hydrotris (3,5-dimethyl-4-X-1-pyrazolyl) borate Ligands [$Tp^{Me2,X}M^{II}(\kappa^2$-O,O′-L)](M = Ni, Co; L = NO_3, OAc; X = Me, H, Br). Bull. Chem. Soc. Jpn 2002, 75, 1255–1262.

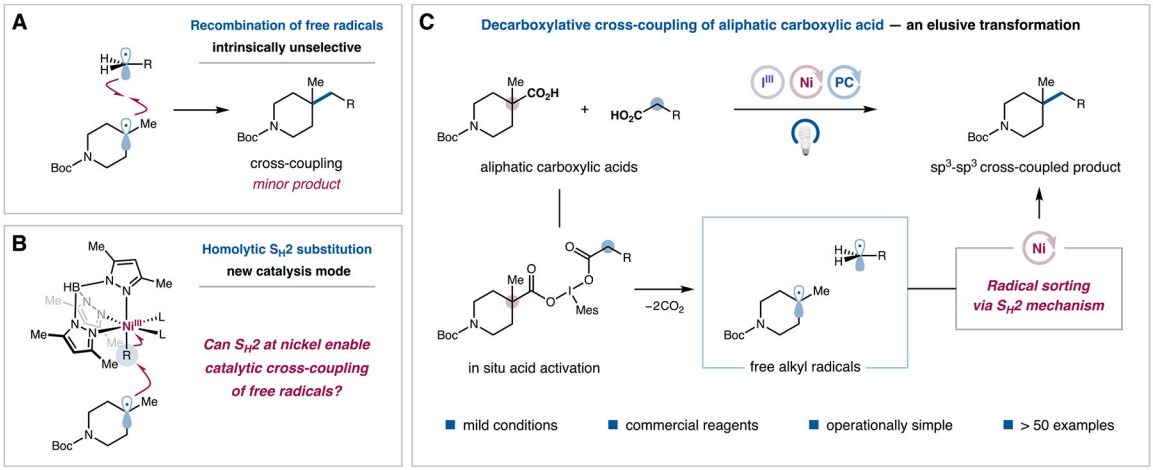

Figure 1.

Project design. (A) Recombination of free alkyl radicals is an innately unselective process. (B) Homolytic S_H2 substitution is a new catalytic platform for free radical cross-coupling. (C) Overview of the reaction design. Boc, *tert*-butoxycarbonyl; L, ligand; Me, methyl; Mes, mesityl; PC, photocatalyst

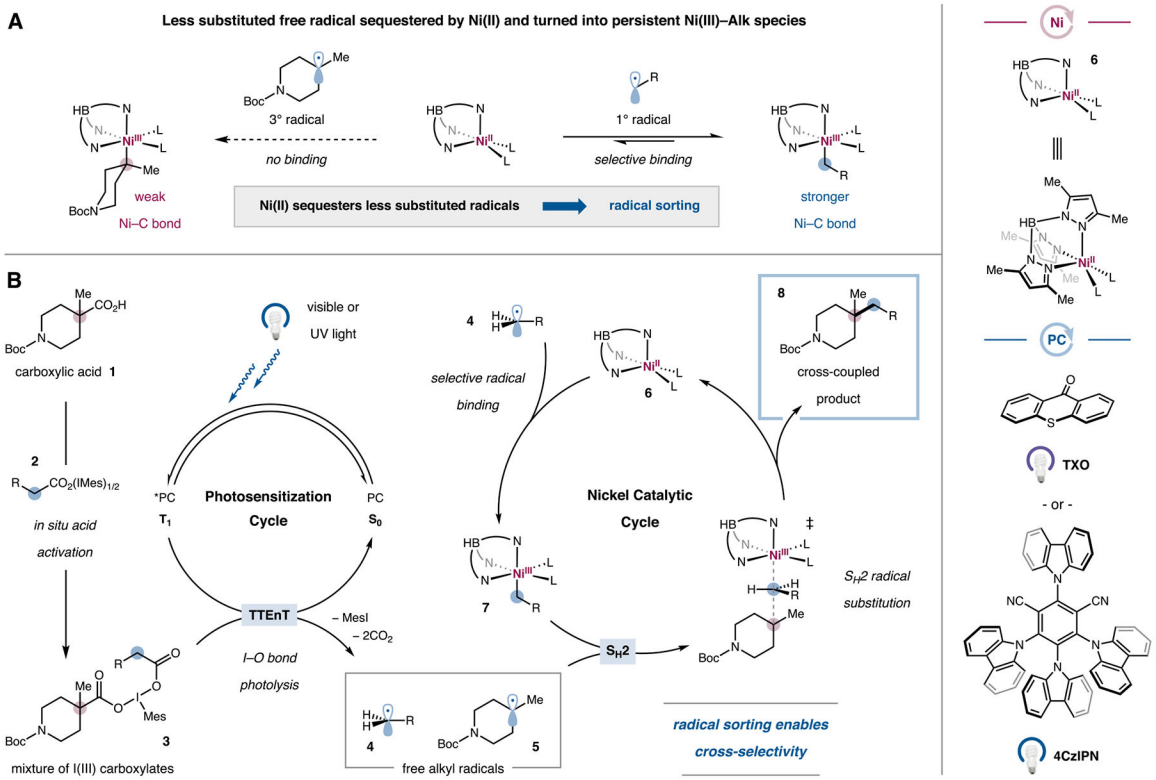

Figure 2.

Design plan for the cross-coupling of carboxylic acids. (A) Radical sorting through selective binding of free radicals to a metal complex.(B) Proposed reaction mechanism. Alk, alkyl; TTEnT, triplet–triplet energy transfer; UV, ultraviolet; 1°, primary; 3°, tertiary.

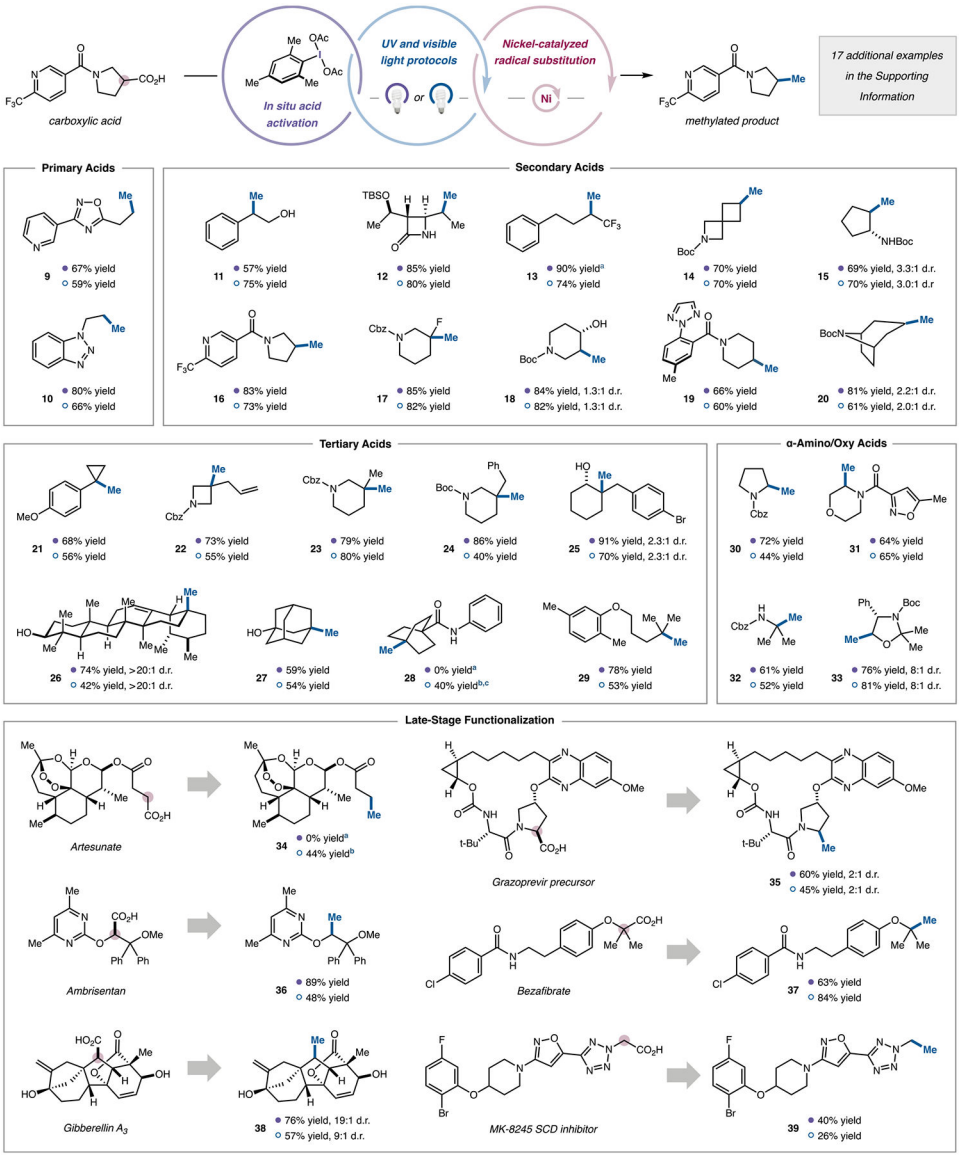

Figure 3.

Scope of the decarboxylative methylation. Purple black circle: UV-light protocol, isolated yields: carboxylic acid (1 mmol), $MesI(OAc)_2$ (2.5 equiv), $Ni(acac)_2$ (5 mol %), K[Tp*] (5 mol %), and TXO (10 mol %) were mixed in Me_2CO_3 (33 mM) and irradiated with 365 nm light for1 h. Blue white circle Blue light protocol, ^1H NMR yield vs 1,3-bis(trifluoromethyl)-5-bromobenzene as an internal standard: carboxylic acid (1 mmol), $MesI(OAc)_2$ (2.5 equiv), $Ni(acac)_2$ (5 mol %), K[Tp*] (5 mol %), and 4CzIPN (5 mol %) were mixed in Me_2CO_3 (33 mM) and irradiated with 450 nm light for 3 h. [a]^1H NMR yield vs 1,3-bis(trifluoromethyl)-5-bromobenzene as internal standard. [b]Isolated yield. [c]5CzBN was used instead of 4CzIPN. 5CzBN, 2,3,4,5,6-penta(carbazol-9-yl)benzonitrile; Cbz, benzyloxycarbonyl; TBS, *tert*-butyldimethylsilyl; *t*-Bu, *tert*-butyl; Ph, phenyl.

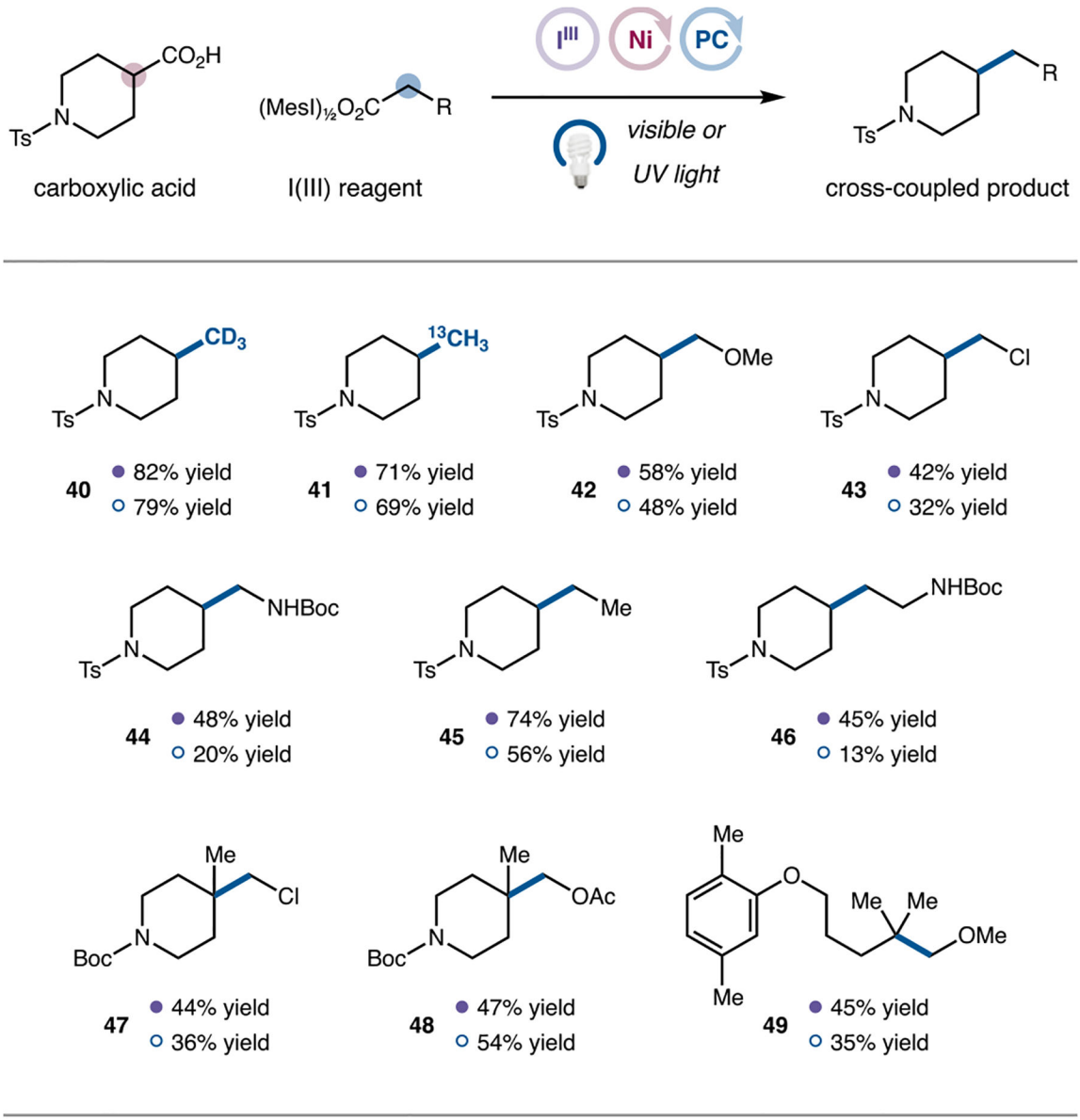

Figure 4.

Scope of carboxylic acid cross-coupling reaction. Purple black circle: UV-light protocol, isolated yields: large-alkyl carboxylic acid (1 mmol), small-alkyl dicarboxylate $MesI(O_2CR)_2$ (2.5 equiv), $Ni(acac)_2$ (5 mol %), K[Tp*] (5 mol %), and TXO (10 mol %) were mixed in Me_2CO_3 (33 mM) and irradiated with 365 nm light for 1 h. Blue white circle: Blue light protocol, ^1H NMR yield vs 1,3-bis(trifluoromethyl)-5-bromobenzene as an internal standard: carboxylic acid (1 mmol), $MesI(O_2CR)_2$ (2.5 equiv), $Ni(acac)_2$ (5 mol %), K[Tp*] (5 mol %), and 4CzIPN (5 mol %) were mixed in Me_2CO_3 (33 mM) and irradiated with 450 nm light for 3 h.

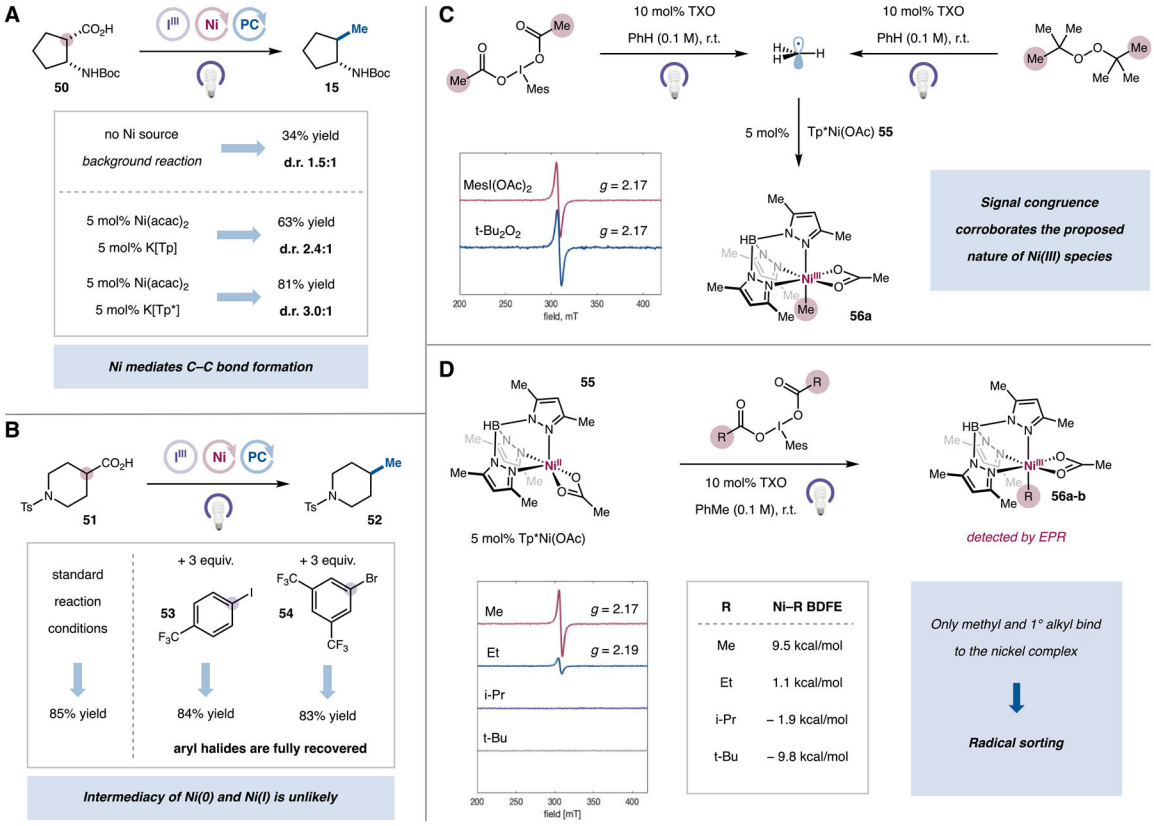

Figure 5.

Mechanistic experiments. (A) Probing nickel involvement in the C−C bond formation step. (B) Probing intermediacy of low-valent Ni species. (C) PhotoEPR detection of Ni(III)−Me species. (D) PhotoEPR experiments to validate radical sorting hypothesis. Ni−R bond dissociation free energies (BDFE) values calculated at SMD(PhMe)-M06-D3(0)/def2-QZVP//TPSS-D3(BJ)/def2-TZVP level of theory. Et, ethyl; *i*-Pr, *iso*-propyl; r.t., room temperature.

Table 1.

Control Experiments for Decarboxylative Methylation

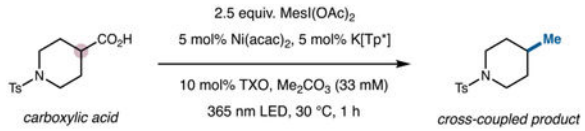

entry[a]	deviation	yield[b] (%)
1	none	85
2	no $Ni(acac)_2$, no K[Tp*]	37
3	no K[Tp*]	51
4	no TXO	82
5	no light	0

[a] 0.1 mmol scale.

[b] UPLC yields vs acetanilide as an internal standard.

See the Supporting Information for further details. Ts, *para*toluenesulfonyl.